Journal of Magnetism and Magnetic Materials 475 (2019) 470–478

Contents lists available at ScienceDirect

Journal of Magnetism and Magnetic Materials

journal homepage: www.elsevier.com/locate/jmmm

Research articles

Magnetic properties and heating efficacy of magnesium doped magnetite nanoparticles obtained by co-precipitation method

Vladan Kusigerski[a,*], Erzsebet Illes[a,1], Jovan Blanusa[a], Saso Gyergyek[b], Marko Boskovic[a], Marija Perovic[a], Vojislav Spasojevic[a]

[a] Condensed Matter Physics Laboratory, The Vinca Institute, University of Belgrade, 11001 Belgrade, Serbia
[b] Department for Materials Synthesis, Jozef Stefan Institute, 1000 Ljubljana, Slovenia

ARTICLE INFO

Keywords:
Nanostructured materials
Oxide materials
Ferrofluids
Magnetic properties
Magnetic hyperthermia

ABSTRACT

Ferrofluids based on magnesium substituted magnetite nanoparticles $Mg_xFe_{3-x}O_4$ (x = 0.1; 0.2; 0.4) were synthesised by a chemical co-precipitation method. Their physical properties have been compared with those of the magnetite based ferrofluid obtained by the same synthesis route. Both XRD and TEM studies showed particle size decrease with the increased Mg content while DLS experiments pointed to the more prominent aggregation of Mg-containing nanoparticles. Magnetic properties investigation conducted on the powder (i.e. dried) specimens showed decrease of magnetization values with increased Mg content except for the lowest concentration of x = 0.1 where substantial saturation magnetization rise of about 40% was recorded at room temperature. Heating abilities of the studied ferrofluids under the applied AC fields (SAR values) also showed decreasing trend with the increased Mg content even for x = 0.1 sample despite its elevated magnetization value. This trend has been understood as a consequence of the changed intrinsic nanoparticle properties such as size and magnetic anisotropy, as well as contribution of a collective behaviour due to an increased nanoparticle aggregation in Mg-doped systems.

1. Introduction

Nanoparticle magnetic materials have provoked an enormous research interest in the last few decades due to the emergence of new magnetic phenomena compared to their bulk counterparts. Properties like superparamagnetism, increased anisotropy (i.e. high coercivity), exchange bias (intra-particle interactions), and collective phenomena (inter-particle interactions) proved to be of interest regarding both basic science and vast number of technological applications including biomedicine, data storage, magnetic sensing, environmental remediation, etc. [1–3].

Due to the reduction of a particle size down to a typical size of biological entities the application of magnetic nanomaterials in biomedicine is considered among the most promising ones, comprehending cell separation, contrast agents, targeted drug delivery, magnetic hyperthermia, tissue engineering, magnetic biosensors, etc. [4–7]. For these applications stable suspension of magnetic nanoparticles in a liquid medium is required, commonly referred to as magnetic colloid or ferrofluid. Of a critical importance for clinical use in diagnostics and therapy is material biocompatibility, and so far iron-oxides based materials are the only FDA and EMA approved[2] magnetic nanomaterials for such purposes [8]. Among all iron-oxides, magnetite Fe_3O_4 and maghemite (γ-Fe_2O_3) have been most thoroughly studied so far due to their superior magnetic properties [9,10].

On the other hand, particle nanosizing can also cause a certain drawbacks among which the most important is a magnetization reduction due to the existence of a disordered nanoparticle surface layer, usually referred to as a particle shell [11]. One possibility to compensate for this reduction is to increase intrinsic magnetization of the material by controlling its composition and/or its crystal structure parameters. Well known materials convenient for such manipulations are spinel ferrites with chemical formula $(X^{2+}_{1-\delta}Fe^{3+}_{\delta})[X^{2+}_{\delta}Fe^{3+}_{2-\delta}]O_4$, where X denotes divalent cation while parentheses and square brackets denote tetrahedral A and octahedral B crystal sites, respectively [12]. Cation inversion degree δ can take any value in the range $0 < \delta < 1$, where 0 and 1 denotes normal or inverse spinel, respectively. Magnetism of spinel ferrites is determined by both cation composition and their distribution over A and B sites (i.e. inversion degree δ), and thus

* Corresponding author.
E-mail address: vladank@vinca.rs (V. Kusigerski).
[1] Present address: Department of Physical Chemistry and Materials Science, University of Szeged, H-6720 Szeged, Hungary.
[2] FDA - Food and Drug Agency; EMA - European Medicines Agency.

https://doi.org/10.1016/j.jmmm.2018.11.127
Received 15 August 2018; Received in revised form 26 October 2018; Accepted 29 November 2018
Available online 30 November 2018
0304-8853/

many research studies have been devoted to correlations between these parameters and magnetic properties. In case of a nanoparticle magnetite, which in ideal case is considered as an inverse spinel $(Fe^{3+})[Fe^{2+}Fe^{3+}]O_4$, numerous investigations were dealing with partial substitution of iron ions for a variety of other ions: magnetic 3d ions (Ni, Co, Mn, V) [13–18] or 4f ions (Gd, Dy, Ho, Tm, Yb) [19,20], or nonmagnetic (i.e. diamagnetic) ions (Y, Ga, Zn) [21–24]. In addition, for the preparation of the above mentioned compounds many different synthesis techniques have been applied, including co-precipitation, thermal decomposition, mechanochemistry, hydrothermal route, sol-gel, and microemulsion [13–24]. Direct comparison of the obtained results is difficult since the applied synthesis method has a decisive impact on both cation distribution and nanoparticle size, and they both influence magnetic properties. This is especially true in case when magnetic ions are used as dopants since their magnetic moments and exchange interaction affinities become additional parameters that should be taken into account.

In case of nonmagnetic ions doping, it turns out that a notable increase of magnetization could be obtained in case of preferential occupation of tetrahedral sites by a substituent cations, and so far the best results have been achieved in case of Zn^{2+} [23,25] and Ga^{3+} [22] ions. In contrast, magnetization reduction has been observed for Y^{3+} ions which preferentially occupy octahedral sites in the spinel structure [21]. These results could be understand by adopting the simple model of Néel [26] in which magnetic ordering of spinels is governed by A-O-A, A-O-B and B-O-B superexchange interactions only. These interactions force an antiparallel spin orientation of iron ions, so Fe^{3+} atoms in A and B sites of magnetite compensate each other, and consequently the net magnetization originates from uncompensated Fe^{2+} moments. By replacing part of Fe^{3+} ions by diamagnetic ions number of uncompensated spins increases thus elevating the net magnetization of the system.

Magnesium ion Mg^{2+} is a promising candidate for Fe_3O_4 doping because its ionic radius in tetrahedral surrounding (0.57) is closer to A-site Fe^{3+} radius (0.49) compared to tetrahedral Zn^{2+} radius (0.60) [27] while biocompatibility reasons further justify its convenience. Studies of the nanoparticle magnesium ferrite $MgFe_2O_4$ have shown that the degree of inversion depended on the synthesis method, and that it might be influenced by processing parameters [28–30]. At the same time heating performances in the applied AC fields also depended on the synthesis pathway, and in some cases they were superior compared to nanoparticle magnetite. However, despite promising properties of Mg^{2+} ion, to our best knowledge there has been just a single research devoted to magnesium doping of nanosized magnetite with the focus on its applicability as anode material in lithium batteries [31].

In this work we have investigated effects of magnesium substitution for iron in nanoparticle magnetite $Mg_xFe_{3-x}O_4$ obtained by a chemical co-precipitation for three concentrations x = 0.1, 0.2 and 0.4. Research comprehended samples' structure/microstructure, magnetic properties and heating efficacy in AC magnetic fields, with the magnetic hyperthermia as a targeted application in mind.

2. Experimental

All studied samples (magnetite and Mg doped magnetite with various magnesium content) were synthesized by a chemical reverse co-precipitation method. Analytical grade chemicals, $MgSO_4$*7 H_2O (Merck), $(NH_4)_2Fe(SO_4)_2$*6 H_2O (Sigma-Aldrich), $FeCl_3$*6 H_2O (Sigma-Aldrich) and NaOH (Carlo Erba) were used. Calculated amounts of $MgCl_2$, $(NH_4)_2Fe(SO_4)_2$ and $FeCl_3$ were dissolved in 10 mL of distilled water in separate beakers, then mixed together and added to tempered 0.4 M NaOH solution during vigorous stirring. Firstly, few drops of the mixture of the metal salts were put to induce the nucleus formation, and then the whole volume of the solution was slowly poured into the balloon. The slurry was kept at 80 °C for 2 h under continuous stirring. After cooling the mixture down to room temperature, the formed dark brown product was washed several times with distilled water combined with magnetic separation. Finally the pH of the slurry was set down to pH ~ 2 and the nanoparticles were dialysed against 0.001 M HCl solution to eliminate the excess salt left from the synthesis. The final product was stored in ferrofluid form in a fridge at pH ~ 4 until further use. Samples were labelled as S0, S10, S20 and S40, according to their Mg-content of 0, 10, 20 and 40%, respectively. The concentration of each suspension was determined by gravimetric method and found to be 8.80, 3.10, 3.13, and 9.20 g/l for samples S0, S10, S20 and S40, respectively. The powder counterparts of the studied samples were obtained by drying the synthesized suspensions.

To investigate crystal structure and phase composition of the obtained samples powder X-ray diffraction data were recorded in Bragg-Brentano geometry on a Rigaku Smartlab 3 kW powder diffractometer. The setup included Cu $K\alpha_{1/2}$ radiation, passive Ni-filter, 0.5° divergent slit, and DTex Ultra 250 detector. The DTex detector was used in narrow energy gap mode in order to suppress iron fluorescence background originating from the copper radiation. The so-collected X-ray diffraction data were analyzed by using FullProf program [32] in profile matching mode (LeBail fit). For particle size estimation, instrumental broadening (resolution function) was extracted from LaB_6 standard diffraction pattern.

Particle size and morphology were investigated by using JEOL-JEM 2100 high resolution transmission electron microscope operating at 200 KV. In the process of samples preparation for TEM ferrofluids were first diluted by 0.001 M HCl solution in order to prevent particle aggregation by keeping the suspension pH in the acidic region. The so-diluted solutions were deposited on a nickel supported carbon film and dried in air. Besides recording TEM micrographs, SAED images were also made to check a crystal phase purity.

The pH-dependent surface charging, the hydrodynamic size and particle aggregation of the studied samples were characterized by Malvern ZetaSizer NANO ZS90 device which utilizes 90° scattering optics and a 4 mW He-Ne laser source (λ = 633 nm). Hydrodynamic size was determined by dynamic light scattering (DLS) using polystyrene cuvettes in dilute sols of ferrofluids from pH ~ 3 up to pH ~ 10 in the presence of 10 mM NaCl. The pH was adjusted by adding 0.01 M HCl or NaOH solutions. Z-average hydrodynamic diameter and polydispersity index (PDI) were obtained by cumulant analysis of the correlation function. Electrokinetic potential measurements were performed by laser Doppler electrophoresis on the same samples using in DTS 1071 disposable zeta cells. The Zetasizer software automatically calculated the zeta potentials from the measured electrophoretic mobility values applying the Smoluchowski equation, assuming, that $K{\cdot}a >> 1$ (where K and a are the Debye-Hückel parameter and particle radius, respectively). The accuracy of the electrokinetic potential determination was ± 5 mV.

Magnetic measurements comprehending temperature dependence of magnetization in a zero-field-cooled (ZFC) and field-cooled (FC) regimes as well as field dependence of isothermal magnetization were done on a commercial SQUID-based magnetometer Quantum Design MPMS XL-5. Research on the heating abilities of the investigated ferrofluids under the applied AC magnetic fields has been performed on a commercial nB nanoScale Biomagnetics DM1 device equipped with the fibre optics temperature sensor. Measurements of the ferrofluid temperature change with time were made under non-adiabatic conditions in a wide range of field amplitudes (50–300 Oe) and frequencies (252–808 kHz).

3. Results and discussion

3.1. 1 Crystal structure and morphology

The recorded X-ray diffraction patterns are presented in Fig. 1.a, which confirms that reflections broadening were proportional to Mg content. All diffraction peaks were indexed within magnetite spinel

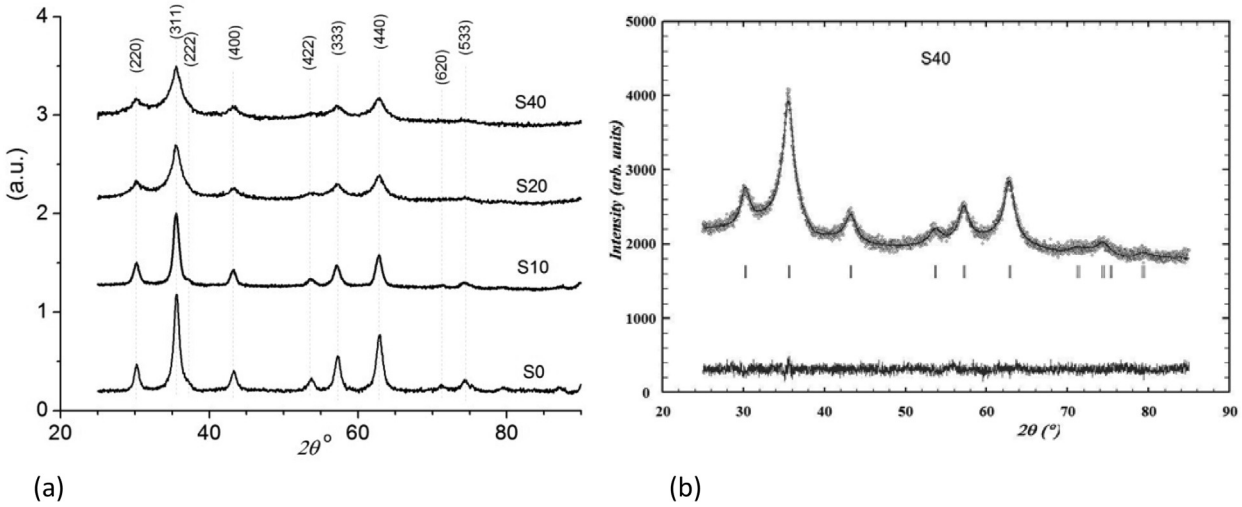

Fig. 1. Diffraction patterns for $Mg_xFe_{3-x}O_4$ samples: (a) Broadening of the diffraction peaks with the increasing Mg content; (b) Refined pattern (line) and experimental data (symbols) for x = 0.40 sample: line at the bottom represents the difference between experimental and calculated values.

Table 1
Cell parameter a and average domain size D obtained by refinement of X-ray powder data for $Mg_xFe_{3-x}O_4$ samples. Particle sizes determined from TEM micrographs (see text) are given in the last column.

Sample	a (Å)	D (nm) – XRD	D (nm) – TEM
S0	8.359(1)	7.8(9*)	10 (2)
S10	8.366(1)	6.1(1.7*)	9 (2)
S20	8.368(2)	3.8(9*)	7 (2)
S40	8.369(1)	3.4(7*)	6 (2)

* Represents the degree of anisotropy, not the standard deviation.

structure (space group Fd-3 m), and no other phases have been observed. As an example, one of the refined patterns (for x = 0.4) is shown separately in Fig. 1.b. The obtained cell parameters and particle sizes from LeBail fit are summarized in Table 1.

By inspection of Table 1 it could be noticed that the biggest difference in cell parameter *a* is between S0 and S10 samples. The magnitude of this change diminishes with Mg content increase and becomes almost negligible for samples S20 and S40. The average domain size D decreases from about 8 nm for S0 sample to below 4 nm for S40 sample. Such a drop in particle size by iron substitution in magnetite has been already reported in several cases for different dopant ions, such as Zn [23,25], Mg [31], Y [21] and Ni [14]. In addition, the certain degree of anisotropy found over different crystallographic directions suggests that particles slightly deviate from spherical shape, which is also confirmed by TEM observations (see below).

TEM micrographs of samples S0, S10 and S20 with corresponding selected area electron diffraction (SAED) patterns are shown in Fig. 2(a)–(c), respectively. Reduction of nanoparticle size with increasing Mg content is apparent, while the average particle size and size distribution were determined by using the imageJ program. The diameter of at least 100 particles per sample was measured and fitted to a log normal distribution (insets in TEM micrographs in Fig. 2). The so-obtained average diameters and standard deviations are given in Table 1 from which the wide size distribution of particles could be seen. Bigger particle diameters obtained by TEM compared to XRD findings is not uncommon, and it is usually ascribed to poorly crystallized layer on the particle surface. It could be also noticed that nanoparticle shapes span from almost spherical to simple polyhedrons, which is in line with the X-ray findings on the crystalline anisotropy, also given in Table 1. SAED patterns confirm that crystal structure is of the cubic spinel type for all the samples without presence of other crystal phases.

3.2. Hydrodynamic size, surface charging and particle aggregation

Intensity distribution of particle sizes obtained from DLS experiments at pH ~ 4 are shown in Fig. 3, while maximums of hydrodynamic diameter values together with Z-average hydrodynamic diameters and PDI values are summarized in Table 2. All Mg-doped samples showed larger average hydrodynamic diameter (above 100 nm) compared to the non-substituted one (~44 nm), although the PDI values remained constant (~0.2) thus indicating a moderate polydispersity of the nanoparticles. The largest hydrodynamic diameter was obtained for S20 sample. Literature data is scarce but we could compare the obtained values for Mg substituted samples to the hydrodynamic diameter of approximately 146 nm determined for magnesium ferrite [33].

In aqueous media metal oxide nanoparticles are hydrated, and amphoteric ≡Me-OH surface sites may exist on their surface in protonated or deprotonated state depending on the pH of the system [34]. This can be represented as:

$$\equiv Me - OH + H^+ \rightleftharpoons \equiv Me - OH_2^+ \quad (1)$$

$$\equiv Me - OH \rightleftharpoons \equiv Me - O^- + H^+ \quad \text{or} \quad \equiv Me - OH + OH^- \rightleftharpoons \equiv Me - O^- + H_2O \quad (2)$$

where Me stands for either iron or magnesium. The pH-dependent surface charging of S0 and S10 ferrofluid samples studied from pH ~ 3 up to pH ~ 10 in the presence of 10 mM NaCl can be seen in Fig. 4. It can be seen that nanoparticles in both samples have positive charge below pH ~ 7, while they are negatively charged above pH ~ 8. At low pHs positively charged $\equiv Me–OH_2^+$ sites form due to the protonation of the surface sites. An increase of pH leads to gradual decrease of the zeta potential and it becomes zero around pH ~ 8, indicating the isoelectric point (IEP), i.e. the pH value where the charge reversal takes place. At pHs higher than ~8 the zeta potential is negative, because the surface active sites are deprotonated and $\equiv Me–O^-$ sites are present on the particle's surface. For undoped magnetite the pH_{IEP} was ~7.9 which is in good accordance with the published data [34,35], while moderate reduction down to ~7.3 could be observed for S10 sample. Similar reduction of pH_{IEP} was obtained for Mg-ferrite with approximately 10% Mg content [36]. The reduced pH_{IEP} could be explained by the presence of Mg, since for nanoparticle Mg-ferrite a value of pH_{IEP} ~7 was observed [33].

The pH-dependent aggregation behaviour of S10 sample follows the change of the zeta potential as shown in Fig. 4. Far from the pH_{IEP} value (i.e. in the range 3 < pH < 5) the measured size is about 120 nm due to the electrostatic stabilization arising from the strong repulsion

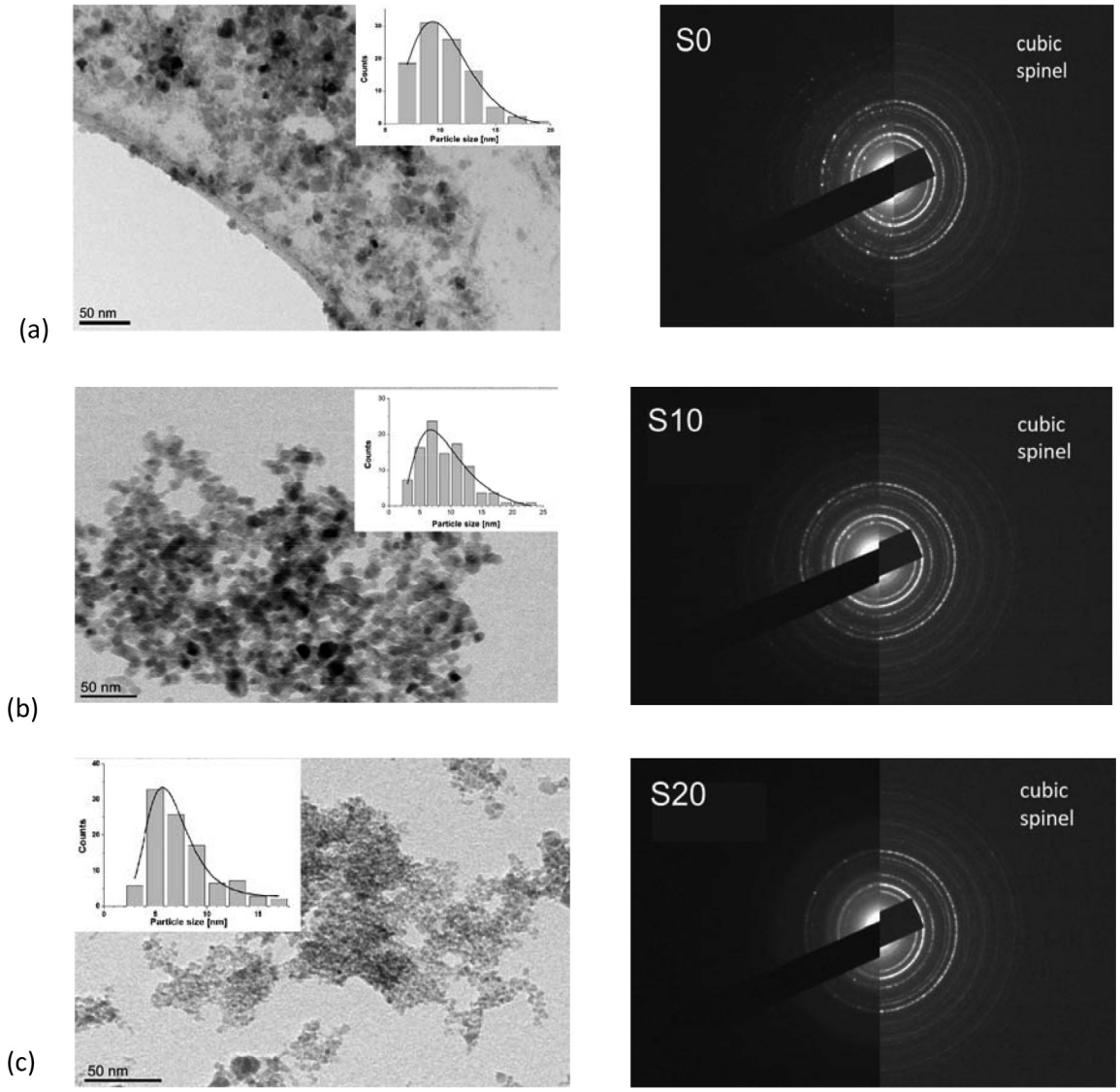

Fig. 2. TEM micrograph and respective SAED patterns for samples S0 (a), S10 (b) and S20 (c). Insets in TEM micrographs represent particle size distributions while lines show best fit to a log-normal distribution.

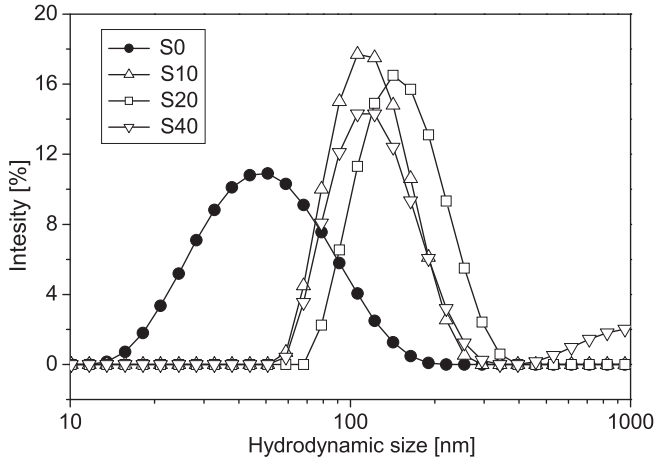

Fig. 3. Intensity distribution of particle hydrodynamic sizes obtained by DLS experiments on ferrofluid samples at pH ~ 4.

Table 2
Hydrodynamic parameters of investigated samples obtained from DLS experiments at pH ~ 4. HD denotes hydrodynamic diameter maximum with standard deviation given in parentheses.

Sample	Z-Average [nm]	PDI	HD [nm]
S0	44	0.20	52 (24)
S10	112	0.13	122 (37)
S20	149	0.17	162 (59)
S40	134	0.25	124 (41)

between the highly positively or negatively charged particles. Around the IEP (i.e. in the range from pH ~ 6 to ~ 9) the absolute value of the electrokinetic potential is small (or zero), which leads to particle aggregation resulted in large size values (> 1000 nm) and thus pointing to the compromised ferrofluid stability.

3.3. Static magnetic properties

Magnetic field dependence of isothermal magnetization of the powder specimens recorded at the room temperature is shown in Fig. 5a. Coercive field values H_C of all the samples are less than 10 Oe

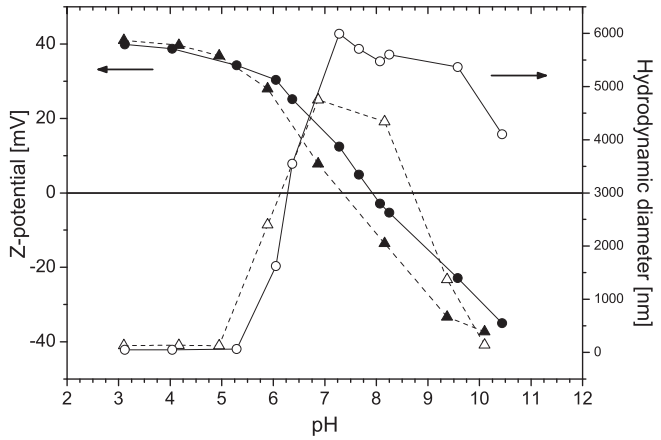

Fig. 4. Electrokinetic potential (full symbols) and hydrodynamic particle size (empty symbols) of S0 (circles) and S10 (triangles) ferrofluid samples as the function of pH.

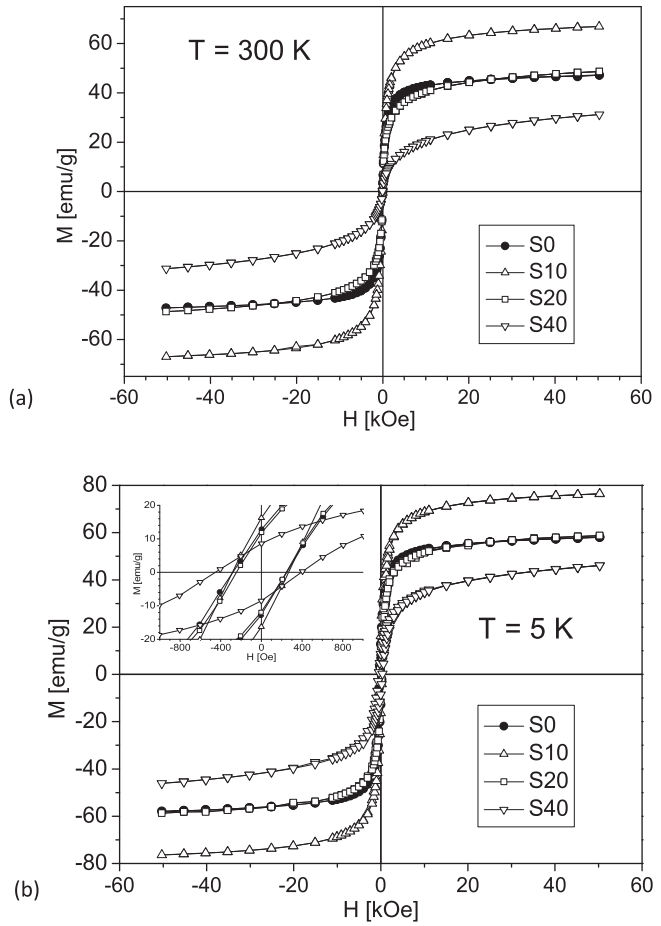

Fig. 5. Field dependence of the isothermal magnetization for powder $Mg_xFe_{3-x}O_4$ samples: (a) Room temperature data; (b) Data recorded at 5 K temperature - inset shows low field behaviour of M(H) curves.

which is in the range of a remnant field of superconducting magnets in QD MPMS device [37]. This points to superparamagnetic nature of all the samples at room temperature. Magnetization of the sample S10 is considerably higher compared to the undoped S0 sample, and the increase of its value at the maximum field of 5 T is about 40% (Table 3). This value decreases with Mg content, and for S40 sample it drops for 34% in respect to S0.

M(H) dependencies recorded at the temperature of 5 K are shown in Fig. 5b. Their behaviour at higher field values resembles the room temperature pattern i.e. while the considerable magnetization increase is obtained for S10 sample magnetization values of samples with higher dopant content experience decrease. All magnetization curves display hysteretic behaviour with almost constant coercive field value H_C of about 250 Oe except in the case of S40 sample where H_C increases up to 400 Oe. This result, together with the fact that high field values of magnetization for S40 show more pronounced departure from saturation, point to the increased anisotropy present in this sample. Existence of magnetic hysteresis indicates that all investigated nanoparticle systems are either in the blocked or frozen state at low temperatures.

Table 3
Important parameters of the investigated samples obtained from magnetic measurements.

Sample	T_{max} [K]	T_{irr} [K]	M_{5T} (5 K) [emu/g]	H_C (5 K) [Oe]	M_{5T} (300 K) [emu/g]	H_C (300 K) [Oe]
S0	218	270	58	250	47	~0
S10	212	255	76	270	67	~0
S20	140	275	59	240	49	~0
S40	86	230	46	400	31	~0

To investigate the temperature dependence of magnetization we have performed magnetization vs. temperature measurements in both ZFC and FC regimes in the field of 100 Oe. Results are shown on Fig. 6. where it can be seen that all ZFC curves possess maximum (denoted for each curve) whose position T_{max} shifts to lower temperatures with the increased Mg concentration. At the same time, values of mass magnetization increases for samples S10 and S20 compared to S0 sample while considerable decrease occurs for S40 specimen.

It has been established in many researches that the value of blocking temperature T_B diminishes with the nanoparticle size reduction [38,39]. Thus, if we consider position of a maximum in ZFC magnetization curve as a T_B value then its decrease with the Mg content is in line with the concomitant particle size reduction already revealed in previous paragraphs by other experimental techniques. Consequently, the magnetization increase for samples S10 and S20 despite the particle size reduction is a result of the intrinsic magnetization rise due to the Mg doping. This points to the predominant distribution of Mg^{2+} ions in tetrahedral positions in these two samples. In addition, the considerable magnetization reduction obtained for S40 together with the increased anisotropy (as found from M(H) measurements) may be an indication that for this dopant concentration Mg^{2+} ions occupy octahedral positions in an elevated percentage.

Temperature at which bifurcation between ZFC and FC curves

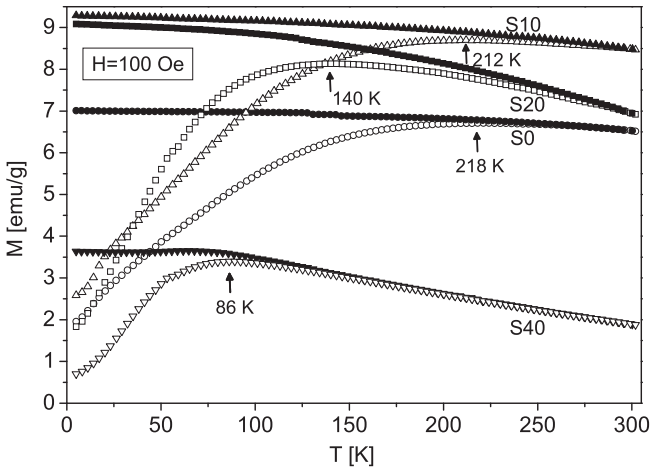

Fig. 6. Temperature dependence of mass magnetization in 100 Oe field in ZFC (empty symbols) and FC (full symbols) regimes for powder $Mg_xFe_{3-x}O_4$ samples. Position of a maximum in ZFC regime is denoted for each curve.

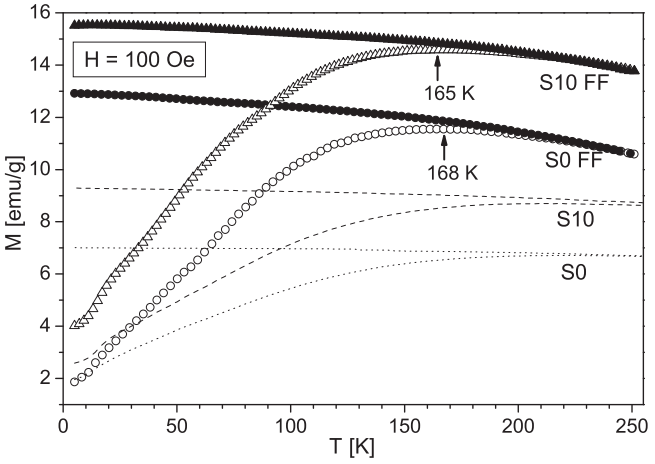

Fig. 7. ZFC-FC data (symbols) in 100 Oe field for ferrofluid counterparts of samples S0 and S10 (denoted by S0 FF and S10 FF, respectively) in their frozen state (temperature region 5–250 K). Data for powder S0 and S10 samples (dotted and dashed lines, respectively) are given for comparison.

occurs is usually referred to as irreversibility temperature T_{irr}, and it is commonly accepted that its value is determined at the point where the condition $(M_{FC}\text{-}M_{ZFC})/M_{FC} < 1\%$ is fulfilled. Values of T_{irr} obtained by applying this condition are listed in Table 3, and it can be seen that all of them are below the room temperature. Since T_{irr} is considered as the blocking temperature of the largest nanoparticles in the system [40], we may conclude that the obtained irreversibility temperatures additionally point to superparamagnetic behaviour of all the samples at room temperature.

FC magnetization curves of all samples show "flatness" i.e. they undergo a very slow increase with the temperature reduction which is a signature of considerable interparticle interactions. This is a common occurrence in a system of "naked" magnetic nanoparticles which are in a close proximity like in powder samples. To check the impact of interparticle interaction on the magnetism of powder samples we have performed ZFC-FC measurements on their ferrofluid counterparts in the frozen state i.e. in the temperature range 5–250 K for samples S0 and S10. Results are depicted in Fig. 7. where also data for powder S0 and S10 samples are indicated for easier comparison. By inspecting this figure three main findings can be drawn: (i) magnetization of ferrofluid samples are considerably higher in respect to dried (powder) counterparts; (ii) position of ZFC maximum for both ferrofluid samples is shifted to lower temperatures in comparison to powder counterparts, and (iii) ration between magnetizations of S1 and S0 in powder form has been preserved in ferrofluids. Based on the above findings we may conclude that interparticle interactions are predominantly of the dipole-dipole type which tend to antiparallely orient particle moments and reduce the net magnetization. These interactions are considerably stronger in powder samples due to the increased proximity of magnetic nanoparticles, and thus net magnetization of dried samples is lower compared to ferrofluide counterparts. Since these findings are the same for both S0 and S10 samples, we can conclude that increase of the magnetization magnitude in S10 sample is not related to interparticle interactions, and so it originates from the Mg doping of S0 sample.

Assuming the homogeneous particle distribution in FF samples and using the mean particle diameters determined by XRD (Table 1) we have estimated the average interparticle distances in investigated ferrofluids (in these calculations density value of 5.17 g/cm^3 for bulk magnetite has been used). The so-obtained values were approximately 60, 80, 60 and 35 nm for samples S0, S10, S20 and S40, respectively. It has been shown in several researches that interparticle distances of even few particle diameters resulted in negligible interparticle interactions [40,41]. This implies that in our suspensions distribution of particles is not homogeneous which is in line with the DLS findings on the presence of particle aggregates in investigated ferrofluids. As already pointed out in Section 3.2, particle aggregation is more pronounced in Mg-doped systems which hydrodynamic radii is about three times bigger compared to undoped S0. Having in mind the above mentioned interparticle distances and decreasing dipole moments due to the particle size decrease with doping, we may conclude that increased aggregation in doped systems is not caused by a dipolar interactions. It rather originates from the changed surface charge of Mg-doped particles i.e. it is predominantly influenced by electrostatic forces in the suspension.

3.4. Magnetic heating in AC fields

Heating abilities in the applied AC fields of the ferrofluid samples under consideration have been evaluated by calculating the Specific Absorption Rate (SAR) value on the basis of the measured temperature vs. time dependences. Since our measurements have been done in non-adiabatic conditions we have used the following expression:

$$SAR = [C_{ps}/m_{NPs}]\cdot|dT/dt|_{t=0} \quad (3)$$

which utilizes time derivative of the temperature at initial time t = 0 [6]. C_{ps} denotes heat capacity of the sample while m_{NPs} represents mass of the dispersed nanoparticles. Since we have been dealing with ferrofluid samples, the value of C_{ps} was related to the specific heat capacity of the dispersion medium C_{pd} and specific heat of nanoparticles C_{pNP} by the expression:

$$C_{ps} = C_{pd}m_d + C_{pNP}m_{NP} \quad (4)$$

For the calculation purposes literature values of the specific heat capacities of water C_{pd} = 4187 J/kgK and of magnetite C_{pNP} = 640 J/kgK [42] were taken into account. The so-obtained SAR values are presented on Fig. 8, where in (a) are shown frequency dependences for the fixed value of field amplitude while (b) represents field dependences for the fixed frequency.

In order to compare the heating efficacy of our samples with the available literature data for similar ferrofluids we have also expressed the obtained SAR values by so-called ILP (Intrinsic Loss Power) values defined as:

$$ILP = SAR/[f\cdot H^2] \quad (5)$$

where f and H denote applied AC field frequency and amplitude, respectively [43]. The ILP has been introduced to allow more direct comparisons of published SAR data by making them independent on AC field parameters. However, the validity of expression (5) also has certain limitations in respect to field parameters and particle size distribution [43]. Consequently, in Table 4 we have compared both SAR and ILP values for our samples with the highest heating efficacy, S0 and S10, with the literature data for ferrofluids based on either magnetite or non-magnetic ion doped magnetite with the similar average core size of MNPs.

Inspection of Table 4 shows that the SAR/ILP values of samples under consideration in this work are comparable with the literature data for similar systems.

From the data presented in Fig. 8 we may see that the highest SAR values were obtained for S0 sample for all applied field amplitudes and frequencies. This result seems surprising, having in mind the obtained values for M_{sat} (Table 3), and considering that SAR is proportional either to M_{sat} (in case of blocked nanoparticle state [48]) or to M_{sat}^2 (in a superparamagnetic region [49]). This is especially noticeable for S10 sample, since its room temperature saturation magnetization is considerably higher than for S0 sample. Also, value of M_{sat} for S20 sample somewhat exceeds the saturation magnetization of S0 sample while its SAR value is several times lower.

To explain the drop in heating performance of Mg doped samples we need to consider both relaxation mechanisms, Néel and Brownian, that contribute to the heat dissipation. The Néel relaxation concerns the

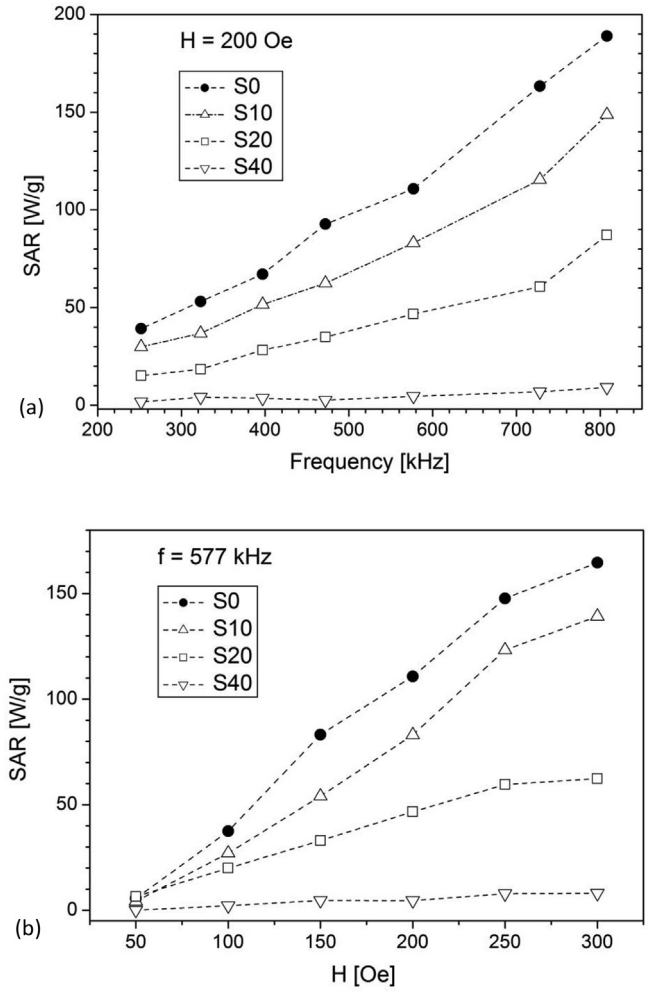

Fig. 8. The obtained SAR values for the investigated ferrofluids at pH ~ 4: (a) frequency dependences for the fixed field amplitude of 200 Oe; (b) field dependences for the fixed frequency of 577 kHz.

fluctuation of the particle's dipolar moment while Brownian relaxation is caused by a mechanical particle rotation in a viscous medium. Relaxation times of these processes are given by $\tau_N = \tau_0 \exp(KV_m/k_BT)$ and $\tau_B = 4\pi\eta r_H^3/k_BT$, for the Néel and Brownian relaxation, respectively [50]. In the above expressions τ_0 denotes so called characteristic time of the material (typically assumed to be in the range 10^{-9}–10^{-10}), K denotes magnetic anisotropy constant, V_m is the nanoparticle magnetic volume, r_H is the particle hydrodynamic radius, and k_B is the Boltzmann's constant.

It is well known that mechanical rotations quickly become insignificant with the increase of the particle hydrodynamic radius since τ_B scales with the cube of r_H [6]. By using the hydrodynamic diameters given in Table 2 (HD values) it is easy to see that τ_B increases for an order of magnitude for Mg doped samples compared to the undoped one thus diminishing the contribution of Brownian relaxation.

Table 5
Values of anisotropy constant K and anisotropy energy KV_m for investigated samples.

Sample	K [10^5 J/m^3]	KV_m [10^{-20} J]
S0	3.0	8.6
S10	6.1	7.3
S20	16.8	4.8
S40	14.4	3.0

Dissipation of thermal energy by the Néel mechanism depends on the KV_m/k_BT ratio, and its contribution is significant only if the magnetic anisotropy energy of the particle is considerably larger than the thermal energy, i.e. if $KV_m \gg k_BT$ [50]. Magnetic volume V_m of the particle could be considered as the volume of the crystallite with the average size determined from the X-ray diffraction (Table 1), while the value of anisotropy constant K is usually determined from the Néel expression $K = 25\ k_BT_B/V_m$ [12], where T_B denotes blocking temperature of the nanoparticle system obtained from ZFC measurement (Table 3). It should be noted that this expression is strictly speaking valid for noninteracting monodisperse magnetic particles only, and so the value of K obtained by applying it in the case of interacting particles is usually overestimated due to the inclusion of the system's collective response [51]. By using the above expression and the corresponding data from Tables 1 and 2 we have determined K and KV_m values, listed in Table 5.

The obtained values of K are at least an order of magnitude higher in comparison to the bulk value for magnetite ($1.35 \cdot 10^4$ J/m^3), and they increase with the nanoparticle decrease, which is a behaviour usually ascribed to the surface effects in nanoparticle material. In contract, anisotropy energy KV_m decrases with Mg doping thus becomes closer to the thermal energy value at room temperature ($\sim 4 \cdot 10^{-21}$ J). This means that the heat dissipation due to the Néel mechanism also diminishes with Mg doping.

Above discussion is restricted to parameters related to individual nanoparticles but we should also consider impact of a collective behaviour on the heating performance of investigated ferrofluids. Namely, magnetic measurements pointed to the existence of dipolar interactions between nanoparticles while DLS results showed increased aggregation of nanoparticles in all ferrofluids based on Mg doped nanoparticles. In aggregated condition distances between magnetic dipoles are much lower which leads to the increased magnetic interactions between them. It has been established in several researches that interparticle interactions influence the heating abilities of the ferrofluid, and this correlation is still a topic of current interest. A comprehensive review on the interparticle interactions impact on heating efficacy is given in [52] while here we will point just to a few typical examples. For instance, by relaying on both experimental data and Monte Carlo simulations of the system of ferromagnetic Fe nanoparticles a decrease of SAR values with the increasing dipolar interactions were found [53]. Similar results have been obtained by numerical simulations [54] and

Table 4
Heating efficacy comparison for ferrofluids based on magnetite or ferrite nanoparticles.

Composition	Core size [nm]	H [kA/m]*	f [kHz]	SAR [w/g]	ILP [nHm^2/kg]	Ref.
Fe_3O_4 (S0)	8	15.9	577	111	0.76	This work
$Mg_{0.1}Fe_{2.9}O_4$ (S10)	6	15.9	577	83.1	0.57	This work
Fe_3O_4	10	24.5	400	130	0.54	[44]
Fe_3O_4	9.5	30	100	29	0.32	[45]
Fe_3O_4	9	27	400	367	1.26	[46]
$MgFe_2O_4$	7	8	279	13.4	1.06	[47]
$Zn_{0.25}Fe_{2.75}O_4$	8.3	6	330	16.65	1.4	[24]

* For easier comparison, one should note that 1 Oe = 79.58 A/m.

by experimental investigations on magnetite based ferrofluids which also pointed to unfavourable role of dipolar interactions on the SAR values [55]. Based on these results we may propose that the increased interparticle interactions due to the elevated aggregation of nanoparticles in Mg doped ferrofluids suppresses heat losses and thus also contributes to the decreasing of SAR values in comparison to the undoped S0 sample.

4. Conclusions

Stable ferrofluids based on the Mg doped magnetite nanoparticles $Mg_xFe_{3-x}O_4$ have been successfully synthesised by utilising chemical reverse co-precipitation method. Powder x-ray study showed than all the samples were of the cubic spinel structure while the cell parameter increased with the magnesium concentration x. TEM photographs revealed the decreasing particle size with increasing amount of Mg, as well as the tendency for particle agglomeration and their deviation from the spherical shape. DLS experiments pointed to the increasing hydrodynamic particle size (up to three times) in doped samples while polydispersity index remained constant.

Study of magnetic properties showed that the significant increase of magnetization occurred only for 10% Mg doping in compare to undoped magnetite sample. By simultaneous comparison of different magnetic parameters (magnetization, coercivity and blocking temperatures) and particle sizes we may conclude that for both 10% and 20% of Mg concentration the intrinsic magnetization increases as a result of Mg doping, while for concentration of 40% the decrease of magnetization occurred. From the viewpoint of Mg ions distribution above results indicate the prevalent occupation of tetrahedral sites in the spinel structure up to 20% of Mg doping while for higher concentrations their distribution over octahedral sites prevails.

Regarding thermomagnetic properties, the best SAR values have been obtained for the ferrofluid based on undoped magnetite nanoparticles, in spite of the increased magnetization of 10% Mg doped sample. To comprehend possible reasons for such a result we have considered both Brownian and Néel contributons to heat dissipation. It has been shown that increased hydrodynamic radii of about three times for Mg-doped systems diminishes the Brownian contribution in these samples. Regarding the Néel contribution, we have found that anisotropy constant K increased with Mg doping while anisotropy energy KV_m had the decreasing trend, approaching the thermal energy value at room temperature. This pointed to diminishing of the Néel contribution with increased Mg content.

Having in mind the existence of dipolar interparticle interactions in investigated systems and increased aggregation in Mg-doped samples we also considered the impact of the collective phenomena on the obtained SAR values. The results published so far showed that increased interparticle interactions usually diminished heating abilities in AC fields. Thus we may conclude that elevated aggregation in Mg-doped systems acted as additional impeding factor regarding magnetic heating.

Our results show that magnesium substitution for iron in nanoparticle magnetite up to 20% of Mg leads to intrinsic magnetisation increase. In contrast, heating abilities of the ferrofluids based on Mg-doped nanoparticles is lower compared to the one based on pure magnetite thus giving the advantage to the latter as heating agent for magnetic hyperthermia. However, considerably enhanced magnetization of 10% Mg doped magnetite as well as its superparamagnetic behaviour at room temperature recommends it as a convenient material for different applications based on magnetic separation or external field targeting.

Acknowledgements

The authors gratefully acknowledge support provided by the project III-45015 funded by the Serbian Ministry of Education, Science and Technological Development, EU funded project FP7-EraChairs-MAGBIOVIN, and COST Action TD1402-RADIOMAG.

References

[1] R. Skomski, Nanomagnetics, J. Phys.: Condens. Matter 15 (2003) R841–R896.
[2] G.C. Papaefthymiou, Nanoparticle magnetism, Nano Today 4 (2009) 438–447.
[3] Nanomagnetism: Fundamentals and Applications, Volume 6, 1st Edition, Series Volume Editor: Chris Binns, Elsevier, 2014.
[4] V.K. Varadan, L.F. Chen, J. Xie, Nanomedicine: Design and Applications of Magnetic Nanomaterials, Nanosensors and Nanosystems, Wiley, 2008.
[5] Nguyen T.K. Thanh (Ed.), Magnetic Nanoparticles: From Fabrication to Clinical Applications, CRC Press, Taylor & Francis Group, Boca Raton, FL, 2012.
[6] E.A. Périgo, G. Hemery, O. Sandre, D. Ortega, E. Garaio, F. Plazaola, F.J. Teran, Fundamentals and advances in magnetic hyperthermia, Appl. Phys. Rev. 2 (2015) 041302.
[7] D.R. Baselt, G.U. Lee, M. Natesan, S.W. Metzger, P.E. Sheehan, R.J. Colton, A biosensor based on magnetoresistance technology, Biosens. Bioelectron. 13 (1998) 731–739.
[8] A.C. Anselmo, S. Mitragotri, Nanoparticles in the clinic, Bioeng. Transl. Med. 1 (2016) 10–29.
[9] S. Chandra, K.C. Barick, D. Bahadur, Oxide and hybrid nanostructures for therapeutic applications, Adv. Drug Deliv. Rev. 63 (2011) 1267–1281.
[10] A. Akbarzadeh, M. Samiei, S. Davaran, Magnetic nanoparticles: preparation, physical properties, and applications in biomedicine, Nanoscale Res. Lett. 7 (2012) 144.
[11] C. Caizer, Nanoparticle Size Effect on Some Magnetic Properties, in: Mahmood Aliofkhazraei (Ed.), Handbook of Nanoparticles, Springer International Publishing, Switzerland, 2015, pp. 1–38.
[12] J.M.D. Coey, Magnetism and Magnetic Materials, Cambridge University Press, New York, 2010 Ch. 11.
[13] S. Larumbe, C. Gómez-Polo, J.I. Pérez-Landazábal, A. García-Prieto, J. Alonso, M.L. Fdez-Gubieda, D. Cordero, J. Gómez, Ni Doped Fe_3O_4 Magnetic Nanoparticles, J. Nanosci. Nanotechnol. 12 (2012) 2652–2660.
[14] G. Rana, U.C. Johri, A study on structural and magnetic properties of Ni-substituted magnetite nanoparticles, J. Alloy. Compd. 577 (2013) 376–381.
[15] H. Zhu, S. Zhang, L.Wu. Yu-Xi Huang, S. Sun, Monodisperse MxFe3−xO4 (M = Fe, Cu Co, Mn) Nanoparticles and Their Electrocatalysis for Oxygen Reduction Reaction, Nano Lett. 13 (2013) 2947–2951.
[16] S.O. Estrada, C.A. Huerta-Aguilar, T. Pandiyan, I.A. Monica Corea, G. Tavizon Reyes-Domínguez, Tuning of the magnetic response in cobalt ferrite $Co_xFe_{3x}O_4$ by varying the Fe^{2+} to Co^{2+} molar ratios: rietveld refinement and DFT structural analysis, J. Alloy. Compd. 695 (2017) 2706–2716.
[17] J. Amighian, E. Karimzadeh, M. Mozaffari, The effect of Mn^{2+} substitution on magnetic properties of $Mn_xFe_{3x}O_4$ nanoparticles prepared by coprecipitation method, J. Magn. Magn. Mater. 332 (2013) 157–162.
[18] V.L. Pool, M.T. Kleb, C.L. Chorney, E. Arenholz, Y.U. Idzerda, Enhanced magnetization in $V_xFe_{3x}O_4$ nanoparticles, J. Magn. Magn. Mater. 396 (2015) 304–307.
[19] Z. Cvejic, B. Antic, A. Kremenovic, S. Rakic, G.F. Goya, H.R. Rechenberg, C. Jovalekic, V. Spasojevic, Influence of heavy rare earth ions substitution on microstructure and magnetism of nanocrystalline magnetite, J. Alloy. Compd. 472 (2009) 571–575.
[20] R.V. Upadhyay, A. Gupta, C. Sudakar, K.V. Rao, K. Parekh, R. Desai, R.V. Mehta, Effect of rare-earth Ho ion substitution on magnetic properties of Fe_3O_4 magnetic fluids, J. Appl. Phys. 99 (2006) 08M906.
[21] M. Mozaffari, J. Amighian, R. Tavakoli, The effect of yttrium substitution on the magnetic properties of magnetite nanoparticles, J. Magn. Magn. Mater. 379 (2015) 208–212.
[22] V.L. Pool, M.T. Klem, C.L. Chorney, E.A. Arenholz, Y.U. Idzerda, Enhanced magnetism of Fe_3O_4 nanoparticles with Ga doping, J. Appl. Phys. 109 (2011) 07B529.
[23] J. Liu, Y. Bin, M. Matsuo, Magnetic Behavior of Zn-Doped Fe_3O_4 Nanoparticles Estimated in Terms of Crystal Domain Size, J. Phys. Chem. C 116 (2012) 134–143.
[24] B. Behdadfar, A. Kermanpur, H. Sadeghi-Aliabadi, M. del Puerto Morales, M. Mozaffari, Synthesis of aqueous ferrofluids of $Zn_xFe_{3x}O_4$ nanoparticles by citric acid assisted hydrothermal-reduction route for magnetic hyperthermia applications, J. Magn. Magn. Mater. 324 (2012) 2211–2217.
[25] J.M. Byrne, V.S. Coker, E. Cespedes, P.L. Wincott, D.J. Vaughan, R.A.D. Pattrick, G. van der Laan, E. Arenholz, F. Tuna, M. Bencsik, J.R. Lloyd, N.D. Telling, Biosynthesis of zinc substituted magnetite nanoparticles with enhanced magnetic properties, Adv. Funct. Mater. 24 (2014) 2518–2529.
[26] L. Neel, Annals Phys. 3 (1948) 137–198.
[27] R.D. Shannon, Revised effective ionic radii and systematic studies of interatomic distances in halides and chalcogenides, Acta Cryst. A 32 (1976) 751–767.
[28] Q. Chen, A.J. Rondinone, B.C. Chakoumakos, Z.J. Zhang, Synthesis of superparamagnetic $MgFe_2O_4$ nanoparticles by coprecipitation, J. Magn. Magn. Mater. 194 (1999) 1–7.
[29] S. Da Dalt, A.S. Takimi, T.M. Volkmer, V.C. Sousa, C.P. Bergmann, Magnetic and Mössbauer behavior of the nanostructured $MgFe_2O_4$ spinel obtained at low temperature, Powder Technol. 210 (2011) 103–108.
[30] M.G. Naseri, M.H.M. Ara, E.B. Saion, A.H. Shaari, Superparamagnetic magnesium ferrite nanoparticles fabricated by a simple, thermal-treatment method, J. Magn. Magn. Mater. 350 (2014) 141–147.
[31] Z. Lv, Q. Wang, Y. Bin, L. Huang, R. Zhang, P. Zhang, M. Matsuo, Magnetic Behaviors of Mg- and Zn-Doped Fe_3O_4 Nanoparticles Estimated in Terms of Crystal Domain Size, Dielectric Response, and Application of Fe_3O_4/Carbon Nanotube

Composites to Anodes for Lithium Ion Batteries, J. Phys. Chem. C 119 (2015) 26128–26142.
[32] J. Rodriguez-Carvajal, T. Roisnel, Line broadening analysis using FullProf: Determination of microstructural properties, Mater. Sci. Forum 443–444 (2004) 123–126.
[33] V.M. Khot, A.B. Salunkhe, N.D. Thorat, R.S. Ningthoujam, S.H. Pawar, Induction heating studies of dextran coated $MgFe_2O_4$ nanoparticles for magnetic hyperthermia, Dalton Trans. 42 (2013) 1249–1258.
[34] E. Tombácz, pH-dependent surface charging of metal oxides, Periodica Polytech., Chem. Eng. 53 (2) (2009) 77–86.
[35] E. Tombácz, A. Majzik, Z.S. Horvat, E. Illes, Magnetite in aqueous medium: coating its surface and surface coated with it, Rom. Rep. Phys. 58 (2006) 281–286.
[36] W. Tang, Su Yu, Qi Li, S. Gao, J.K. Shang, Superparamagnetic magnesium ferrite nanoadsorbent for effective arsenic (III, V) removal and easy magnetic separation, Water Res. 47 (2013) 3624–3634.
[37] Quantum Design: MPMS Application Note 1014-208 A.
[38] J. Chatterjee, Y. Haik, C.J. Chen, Size dependent magnetic properties of iron oxide nanoparticles, J. Magn. Magn. Mater. 257 (2003) 113–118.
[39] H. Shim, P. Dutta, M.S. Seehra, J. Bonevich, Size dependence of the blocking temperatures and electron magnetic resonance spectra in NiO nanoparticles, Solid State Commun. 145 (2008) 192–196.
[40] P. Tartaj, T. Gonzales-Carreno, C.J. Serna, Magnetic behaviour of γ-Fe2O3 nanocrystals dispersed in colloidal silica particles, J. Phys. Chem. B 107 (2003) 20–24.
[41] C. Martinez-Boubeta, K. Simeonidis, M. Angelakeris, N. Pazos-Peres, M. Giersig, A. Delimitis, L. Nalbandian, V. Alexandrikis, D. Niarchos, Critical radius for exchange bias in naturally oxidised Fe nanoparticles, Phys. Rev. B 74 (2006) 054430.
[42] M.W. Chase Jr., NIST-JANAF Themochemical Tables, Fourth Edition, J. Phys. Chem. Ref. Data, Monograph 9 (1998) 1–1951.
[43] M. Kallumadil, M. Tada, T. Nakagawa, M. Abe, P. Southern, Q.A. Pankhurst, Suitability of commercial colloids for magnetic hyperthermia, J. Magn. Magn. Mater. 321 (2009) 1509–1513.
[44] M. Gonzales-Weimuller, M. Zeisberger, K.M. Krishnan, Size-dependant heating rates of iron oxide nanoparticles for magnetic fluid hyperthermia, J. Magn. Magn. Mater. 321 (2009) 1947–1950.
[45] M. Song, Y. Zhang, S. Hu, L. Song, J. Dong, Z. Chen, N. Gu, Influence of morphology and surface exchange reaction on magnetic properties of monodisperse magnetite nanoparticles, Colloids Surf. A 408 (2012) 114–121.
[46] X.L. Liu, H.M. Fan, J.B. Yi, Y. Yang, E.S.G. Choo, J.M. Xue, D.D. Fana, J. Ding, Optimization of surface coating on Fe_3O_4 nanoparticles for high performance magnetic hyperthermia agents, J. Mater. Chem. 22 (2012) 8235–8244.
[47] M.R. Barati, C. Selomulya, K. Suzuki, Particle size dependence of heating power in $MgFe_2O_4$ nanoparticles for hyperthermia therapy application, J. Appl. Phys. 115 (2014) 17B522.
[48] B. Mehdaoui, A. Meffre, L.M. Lacroix, J. Carrey, S. Lachaize, M. Gougeon, M. Respaud, B. Chaudret, Large specific absorption rates in the magnetic hyperthermia properties of metallic iron nanocubes, J. Magn. Magn. Mater. 322 (2010) L49–L52.
[49] R. Hergt, S. Dutz, Magnetic particle hyperthermia – biophysical limitations of a visionary tumour therapy, J. Magn. Magn. Mater. 311 (2007) 187–192.
[50] A.E. Deatsch, B.A. Evans, Heating efficiency in magnetic nanoparticle hyperthermia, J. Magn. Magn. Mater. 354 (2014) 163–172.
[51] V.L. Calero-Diaz del Castillo, C. Rinaldi, Effect of sample concentration on the determination of the anisotropy constant of magnetic nanoparticles, IEEE Trans. Magn. 46 (2010) 852–859.
[52] I.M. Obaidat, B. Issa, Y. Haik, Magnetic properties of magnetic nanoparticles for efficient hyperthermia, Nanomaterials 5 (2015) 63–89.
[53] D. Serantes, D. Baldomir, C. Martinez-Boubeta, K. Simeonidis, M. Angelakeris, E. Natividad, M. Castro, A. Mediano, D.-X. Chen, A. Sanchez, L.I. Balcells, B. Martínez, Influence of dipolar interactions on hyperthermia properties of ferromagnetic particles, J. Appl. Phys. 108 (2010) 073918.
[54] C. Haase, U. Nowak, Role of dipole-dipole interactions for hyperthermia heating of magnetic nanoparticle ensembles, Physical Review B 85 (2012) 045435.
[55] P.H. Linh, P.V. Thach, N.A. Tuan, N.C. Thuan, D.H. Manh, N.X. Phuc, L.V. Hong, Magnetic fluid based on Fe_3O_4 nanoparticles: preparation and hyperthermia application, J. Phys. Conf. Ser. 187 (2009) 012069.